Inorg. Chem. **2005**, *44*, 1580−1587

Control of Electron Acceptor Ability with Ligands (L) in Photoinduced Electron Transfer from Zinc Porphyrin or Zinc Phthalocyanine to $[Ru_3(\mu_3\text{-}O)(\mu\text{-}CH_3COO)_6L_3]^+$

Mitsunari Itou,[†] Midoriko Otake,[†] Yasuyuki Araki,[†] Osamu Ito,*[,†] and Hiroaki Kido[‡]

Institute of Multidisciplinary Research for Advanced Materials, Tohoku University, CREST (JST), Katahira, Aoba-ku, Sendai, 980-8577 Japan, and Department of Materials Chemistry, College of Engineering, Nihon University, Tokusada, Nakagawara, Tamura-machi, Kouriyama, 963-8642 Japan

Received July 7, 2004

Photoinduced electron-transfer processes from the excited triplet states of zinc tetraphenylporphyrin (^{3}ZnTPP*) or zinc tetra-*tert*-butylphthalocyanine (^{3}ZnTBPc*) to oxo-acetato-bridged triruthenium clusters $[Ru_3(\mu_3\text{-}O)(\mu\text{-}CH_3CO_2)_6(L)_3]^+$ have been confirmed by nanosecond laser flash photolysis in the visible and near-IR regions. The rise of the transient absorption spectra of the radical cations of ZnTPP and ZnTBPc and the reduced form of the oxo-acetato-bridged triruthenium cluster ($[Ru_3(\mu_3\text{-}O)(\mu\text{-}CH_3CO_2)_6(L)_3]^0$) were observed with the concomitant decays of ^{3}ZnTPP* or ^{3}ZnTBPc*. The evaluated rate constants (k_{ET}) and quantum yields (Φ_{ET}) for electron-transfer were increased with the order of electron-withdrawing ability of the ligands (L) coordinated to the Ru atoms, 4-cyanopyridine > triphenylphosphine > pyridine > 4-(dimethylamino)pyridine, which is the order of promoting the electron-accepting ability of $[Ru_3(\mu_3\text{-}O)(\mu\text{-}CH_3CO_2)_6(L)_3]^+$. The Φ_{ET} values for ^{3}ZnTPP* were lower than those for ^{3}ZnTBPc*, suggesting the presence of competitive processes such as energy transfer process from ^{3}ZnTPP* to the triplet states of $[Ru_3(\mu_3\text{-}O)(\mu\text{-}CH_3COO)_6(L)_3]^+$. For the back electron-transfer process, second-order kinetics indicates that the radical cations of ZnTPP or ZnTBPc and $[Ru_3(\mu_3\text{-}O)(\mu\text{-}CH_3COO)_6(L)_3]^0$ return to the original system after solvation in polar solvents at a diffusion controlled limit without side reactions, providing reversible photosensitizing intermolecular electron-transfer systems.

Introduction

Photoinduced electron-transfer and energy-transfer processes play a significant role in many inorganic and organic photochemical reactions.[1] The efficient electron-transfer processes based on the smooth redox processes that exist in natural photosynthetic systems control multistep electron-transfer by several factors.[2] Recent developments in photochemistry have led to the achievement of efficient charge separation and long-lived charge-separated states that are controlled by both geometric and energetic factors.[3−8]

* To whom correspondence should be addressed. E-mail: ito@tagen.tohoku.ac.jp. Phone, fax: +81-22-217-5610.
[†] Tohoku University, CREST (JST).
[‡] Nihon University.

(1) (a) Astruc, D. *Electron Transfer and Radical Processes in Transientiton-Metal Chemistry*; VCH Publishers: New York, 1995. (b) Takagi, S.; Inoue, H. *Molecular and Supramolecular Photochemistry*; Ramamurthy, V., Schanze, K. S., Eds.; Marcel Dekker: New York, 1999; Vol. 4, Chapter 6. (c) *Molecular Switches*; Feringa, B. L., Ed.; Wiley-VCH: Weinheim, 2001. (d) O'Regan, B.; Grätzel, M. *Nature* **1991**, *353*, 737−740.
(2) (a) Feher, G.; Allen, J. P.; Okamura, M. Y.; Rees, D. C. *Nature* **1989**, *339*, 111−116. (b) van Grondelle, R.; Monshouwer, R.; Valkunas, L. *Pure Appl. Chem*. **1997**, *69*, 1211−1218.
(3) Kuciauskas, D.; Liddell, P. A.; Lin, S.; Jhonson, T. E.; Weghorn, S. J.; Lindsey, J. S.; Moore, A. L.; Moore, T. A.; Gust, D. *J. Am. Chem. Soc*. **1999**, *121*, 8604−8614.
(4) (a) Imahori, H.; Tamaki, K.; Guldi, D. M.; Luo, C.; Fujitsuka, M.; Ito, O.; Sakata, Y.; Fukuzumi, S. *J. Am. Chem. Soc*. **2001**, *123*, 2607−2617. (b) Imahori, H.; Guldi, D. M.; Tamaki, K.; Yoshida, Y.; Luo, C.; Sakata, Y.; Fukuzumi, S. *J. Am. Chem. Soc*. **2001**, *123*, 6617−6628. (c) Imahori, H.; Tamaki, K.; Araki, Y.; Sekiguchi, Y.; Ito, O.; Sakata, Y.; Fukuzumi, S. *J. Am. Chem. Soc*. **2002**, *124*, 5165−5174. (d) Imahori, H. *Org. Biomol. Chem*. **2004**, *2*, 1425−1433.
(5) Yamazaki, M.; Araki, Y.; Fujitsuka, M.; Ito, O. *J. Phys. Chem. A* **2001**, *105*, 8615−8622.
(6) (a) D'Souza, F.; Deviprasad, G. R.; El-Khouly, M. E.; Fujitsuka, M.; Ito, O. *J. Am. Chem. Soc*. **2001**, *123*, 5277−5284. (b) D'Souza, F.; Smith, P. M.; Zandller, M. E.; McCarty, A. L.; Itou, M.; Araki, Y.; Ito, O. *J. Am. Chem. Soc*. **2004**, *126*, 7898−7907.
(7) Choi, M.-S.; Aida, T.; Luo, H.; Araki, Y.; Ito, O. *Angew. Chem., Int. Ed*. **2003**, *42*, 4060−4063.
(8) Watanabe, N.; Kihara, N.; Furusho, Y.; Takata, T.; Araki, Y.; Ito, O. *Angew. Chem., Int. Ed*. **2003**, *42*, 4060−4063.

10.1021/ic049114s CCC: $30.25
Published on Web 02/02/2005

Chart 1. Molecular Structures

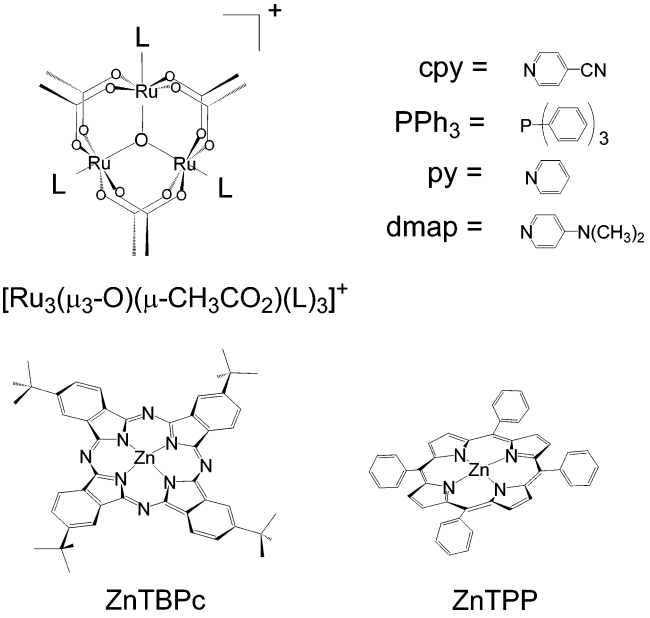

However, further control of the direction and the potential of the electron-transfer systems by using the new redox units is important. Accordingly, metal complexes have tremendous possibilities and advantages, since various properties can be widely controlled by changing the kinds and numbers of metals and ligands. Thus, it is important to systematically explore various factors, which exert various influences upon the electron-transfer processes of metal complexes. Among the metal complexes, multi-metal clusters have recently been widely investigated, including electron-transfer processes in the ground states.[1,2]

For this, the μ-oxo-centered triruthenium clusters bridged by six carboxylate ligands with the general formula of $[Ru_3(\mu_3\text{-}O)(\mu\text{-}CH_3CO_2)_6L_3]^{n+}$ (Chart 1) have been extensively investigated in terms of mixed valence chemistry and catalytic properties.[9−14] This type of cluster complexes shows several characteristic properties in the absorption spectra and electrochemical behavior.[15−17] Recently, it was reported that these cluster complexes form supramolecular architectures by producing oligomers with the bridging ligands.[17−22] In the dimers of triruthenium complexes with bridging ligands, intramolecular electron-transfer processes in the mixed valence states were studied.[23− 25]

In the present study, we report intermolecular photoinduced electron transfer from the triple excited states of zinc tetraphenylporphyrin (^{3}ZnTPP*) or zinc tetra-*tert*-butylphthalocyanine (^{3}ZnTBPc*) used as photosensitizing electron donors to $[Ru_3(\mu_3\text{-}O)(\mu\text{-}CH_3CO_2)_6(L)_3]^+$ as electron acceptors. The direct evidence of electron transfer was obtained by means of laser flash photolysis observing the transient absorption spectra in the visible and near-IR regions. Furthermore, we demonstrate that the control of rate constants (k_{ET}) and quantum yields (Φ_{ET}) via ^{3}ZnTPP or ^{3}ZnTBPc* for photoinduced electron transfer can be achieved by exchanging the terminal ligands (L) as shown in Chart 1 in different polar solvents.

Experimental Section

Materials. Solvents such as acetonitrile (AN), benzonitrile (BN), and *o*-dichlorobenzene (DCB), used for spectroscopic and electrochemical measurements, were all the best grade reagents commercially available. Zinc tetra-*tert*-butyl phthalocyanine (ZnTBPc) was purchased from Aldrich and was subsequently purified by silica gel column using diethyl ether as eluent. Zinc tetraphenylporphyrin (ZnTPP) was synthesized according to the reported methods.[26] Tetra-*n*-butylammonium hexafluorophosphate ($(n\text{-}C_4H_9)_4NPF_6$) used as a supporting electrolyte in the electrochemical measurements was recrystallized from ethyl acetate/benzene (1:1, v/v).[27]

$[Ru_3(\mu_3\text{-}O)(\mu\text{-}CH_3CO_2)_6(EtOH)_3]OAc$, in which the valences of three Ru are (III,III,III), was prepared according to the reported methods.[11] As ligands, commercially available 4-cyanopyridine (cpy), triphenylphosphine (PPh_3), pyridine (py), and 4-(dimethylamino)pyridine (dmap) were employed.

$[Ru_3(\mu_3\text{-}O)(\mu\text{-}CH_3CO_2)_6(cpy)_3]PF_6$. To CH_2Cl_2/CH_3OH (1:1, v/v) solution (20 mL) of $[Ru_3(\mu_3\text{-}O)(\mu\text{-}CH_3CO_2)_6(EtOH)_3]OAc$ (100 mg, 0.115 mmol), cpy (120 mg, 1.15 mmol), and NH_4PF_6 (200 mg, 1.15 mmol) were added and the solution was stirred for 1 day. After evaporation of the solvents to dryness, the residue was dissolved in a minimal amount of CH_2Cl_2. This crude sample solution was placed on a column packed with silica gel (Wakogel C-200) and eluted with using CH_2Cl_2/CH_3OH (99:1, v/v). The first main green fraction was collected and the solvents were evaporated. After the residue was dissolved in a minimal amount of CH_2Cl_2, excess *n*-hexane was added to this solution, obtaining blue-green powders, which were collected by filtration after washing with Et_2O. Yield: 85 mg (65% based on starting $[Ru_3(\mu_3\text{-}O)(\mu\text{-}CH_3CO_2)_6(EtOH)_3]OAc$). Anal. Calcd for $[Ru_3(\mu_3\text{-}O)(\mu\text{-}CH_3CO_2)_6(cpy)_3]PF_6$: C, 31.81; H, 2.85; N, 7.42. Found: C, 32.07; H, 2.59; N, 7.54. ^{1}H

(9) Spencer, A.; Wilkinson, G. *J. Chem. Soc., Dalton. Trans.* **1972**, 1570−1577.
(10) Spencer, A.; Wilkinson, G. *J. Chem. Soc., Dalton. Trans.* **1974**, 786−792.
(11) Baumann, J. A.; Salmon, D. J.; Wilson, S. T.; Meyer, T. J. *Inorg. Chem.* **1978**, *17*, 3342−3350.
(12) Abe, M.; Sasaki, Y.; Nakagawa, A.; Ito, T. *Bull. Chem. Soc. Jpn.* **1992**, *65*, 1411−1414.
(13) Abe, M.; Sasaki, Y.; Yamaguchi, T.; Ito, T. *Bull. Chem. Soc. Jpn.* **1992**, *65*, 1585−1590.
(14) Powel, G.; Richens, D. T. *Inorg. Chim. Acta.* **1993**, *213*, 147−155.
(15) Abe, M.; Sasaki, Y.; Yamada, Y.; Tsukahara, K.; Yano, S.; Yamaguchi, T.; Tominaga, M.; Taniguchi, I.; Ito, T. *Inorg. Chem.* **1996**, *35*, 6724−6734.
(16) Ota, K.; Sasaki, H.; Matsui, T.; Hamaguchi, T.; Yamaguchi, T.; Ito, T.; Kido, H.; Kubiak, C. P. *Inorg. Chem.* **1999**, *38*, 4070−4078.
(17) Abe, M.; Michi, T.; Sato, A.; Kondo, T.; Zhou, W.; Shen, Y.; Uosaki, K.; Sasaki, Y. *Angew. Chem., Int. Ed.* **2003**, *42*, 2912−2915.
(18) Baumann, J. A.; Salmon, D. J.; Wilson, S. T.; Meyer, T. J. *Inorg. Chem.* **1979**, *18*, 2472−2479.
(19) Baumann, J. A.; Wilson, S. T.; Salmon, D. J.; Hood, P. L.; Meyer, T. J. *J. Am. Chem. Soc.* **1979**, *101*, 2916−2920.
(20) Kido, H.; Nagino, H.; Ito, T. *Chem. Lett.* **1996**, 745−746.
(21) Chen, J.-L.; Zhang, L.-Y.; Chen, Z.-N.; Gao, L.-B.; Abe, M.; Sasaki, Y. *Inorg. Chem.* **2004**, *43*, 1481−1490.
(22) Toma, H. E.; Nikolaou, S. *J. Chem. Res. Synop.* **2000**, 326−327.
(23) Ito, T.; Hamaguchi, T.; Nagino, H.; Yamaguchi, T.; Washington, J.; Kubiak, C. P. *Science* **1997**, *277*, 660−663.
(24) Ito, T.; Hamaguchi, T.; Nagino, H.; Yamaguchi, T.; Kido, H.; Zavarine, I. S.; Richmond, T.; Washington, J.; Kubiak, C. P. *J. Am. Chem. Soc.* **1999**, *121*, 4625−4632.
(25) Londergan, C. H.; Salaman, J. C.; Ronco, S.; Kubiak, C. P. *Inorg. Chem.* **2003**, *42*, 926−928.
(26) Adler, A. D.; Longo, F. R.; Finarelli, J. D.; Goldmacher, J.; Assour, J.; Korsakoff, L. *J. Org. Chem.* **1967**, *32*, 476.
(27) Abe, M.; Sasaki, Y.; Yamada, Y.; Tsukahara, K.; Yano, S.; Yamaguchi, T.; Tominaga, M.; Taniguchi, I.; Ito, T. *Inorg. Chem.* **1996**, *35*, 6724−6734.

NMR in $CDCl_3$: δ (ppm) = 1.14 (6H, cpy-*o*), 5.34 (6H, cpy-*m*) and 5.58 (18H, acetate methyl).

$[Ru_3(\mu_3\text{-}O)(\mu\text{-}CH_3CO_2)_6(PPh_3)_3]PF_6$. This compound was obtained by adding PPh_3 and NH_4PF_6 to $[Ru_3(\mu_3\text{-}O)(\mu\text{-}CH_3CO_2)_6(EtOH)_3]OAc$. Yield: 45% based on starting complex. Anal. Calcd for $[Ru_3(\mu_3\text{-}O)(\mu\text{-}CH_3CO_2)_6(PPh_3)_3]PF_6\cdot CH_2Cl_2$: C, 47.61; H, 3.88. Found: C, 47.88; H, 3.79. ^{1}H NMR in $CDCl_3$: δ (ppm) = 5.26 (18H, PPh_3-*o*), 5.80 (18H, acetate methyl), 6.53 (18H, PPh_3-*m*) and 7.40 (9H, PPh_3-*p*).

$[Ru_3(\mu_3\text{-}O)(\mu\text{-}CH_3CO_2)_6(dmap)_3]PF_6$. This compound was obtained by adding dmap and NH_4PF_6 to $[Ru_3(\mu_3\text{-}O)(\mu\text{-}CH_3CO_2)_6(EtOH)_3]OAc$. Yield: 24% based on starting complex. Anal. Calcd for $[Ru_3(\mu_3\text{-}O)(\mu\text{-}CH_3CO_2)_6(damp)_3]PF_6$: C, 33.45; H, 4.08; N, 7.09. Found: C, 33.27; H, 3.89; N, 7.00. ^{1}H NMR in $CDCl_3$: δ (ppm) = 1.75 (6H, dmap-*o*), 2.71 (18H, dmap-methyl), 5.38 (18H, acetate methyl) and 6.19 (6H, dmap-*m*).

Apparatus. ^{1}H NMR spectra were recorded on a JEOL Lambda 400 spectrometer. Chemical shifts were evaluated with respect to an internal reference of TMS in $CDCl_3$.

Steady-state absorption spectra in the visible and near-IR regions were measured on a Jasco V570 DS spectrophotometer. Cyclic voltammetry experiments were carried out using BAS CV-50W voltammetric analyzer at a scan rate of 100 mV s^{-1}. Glassy carbon was used as a working electrode, a platinum wire served as a counter electrode, and an Ag wire (Ag/Ag^+) was used as a reference electrode. The redox potentials were referenced to an internal ferrocene/ferrocenium (Fc/Fc^+) redox couple. All solutions were deoxygenated by bubbling Ar gas through the solutions, to which 0.1 M of $(n\text{-}C_4H_9)_4NPF_6$ was added as a supporting electrolyte.

Nanosecond transient absorption measurements were carried out using a SHG (532 nm) of the Nd:YAG laser (Spectra-Physics, Quanta-Ray GCR-130, fwhm 6 ns) as an excitation source. For transient absorption spectra in the near-IR region (600−1600 nm), monitoring light from a pulsed Xe lamp was detected with a Ge-avalanche photodiode (Hamamatsu Photonics, B2834). Photoinduced events in microsecond time regions were estimated by using a continuous Xe lamp (150 W) and an InGaAs−PIN photodiode (Hamamatsu Photonics, G5125-10) as a probe light and detector, respectively. All the sample solutions in a quartz cell (1 × 1 cm^2) were deaerated by bubbling Ar gas through the solutions for 15 min. Transient absorption measurements were carried out with use of fresh samples, because repeated laser irradiations of ZnTPP and ZnTBPc in the halogenated solvents such as DCB caused substantial color changes.

Results and Discussion

Electrochemical Study. Figure 1 shows the cyclic voltammograms of $[Ru_3(\mu_3\text{-}O)(\mu\text{-}CH_3CO_2)_6L_3]PF_6$ (L = cpy, PPh_3, py, dmap) in AN. All voltammograms show the reversible redox processes. The central peak in the 0 to −1000 mV region was assigned to the reduction potential (E_{red}) of Ru$_3$(III,III,III)/Ru$_3$(III,III,II), which corresponds to $[Ru_3(\mu_3\text{-}O)(\mu\text{-}CH_3CO_2)_6L_3]^+/[Ru_3(\mu_3\text{-}O)(\mu\text{-}CH_3CO_2)_6L_3]^0$.[28−30] Other redox processes were also assigned as depicted in Figure 1.[28−30] The E_{red} values for $[Ru_3(\mu_3\text{-}O)(\mu\text{-}CH_3CO_2)_6L_3]^+/[Ru_3(\mu_3\text{-}O)(\mu\text{-}CH_3CO_2)_6L_3]^0$ are summarized in Table 1, in which the E_{red} values considerably vary with changing the ligands. The E_{red} values are small compared with the E_{red} values expected for Ru(III/II) of mononuclear complex,[31] suggesting appreciable delocalization of electron density among the three Ru atoms in the Ru$_3$(μ_3-O) core.[28,30] It is notable that the E_{red} values depend on the dissociation constants (pK_a) of the ligands against the corresponding conjugate acids of the ligands.[29] Since the pK_a values of the ligands decrease with the electron-withdrawing ability, the E_{red} values shift less negative, indicating an increase in the electron accepting ability of $[Ru_3(\mu_3\text{-}O)(\mu\text{-}CH_3CO_2)_6L_3]PF_6$.

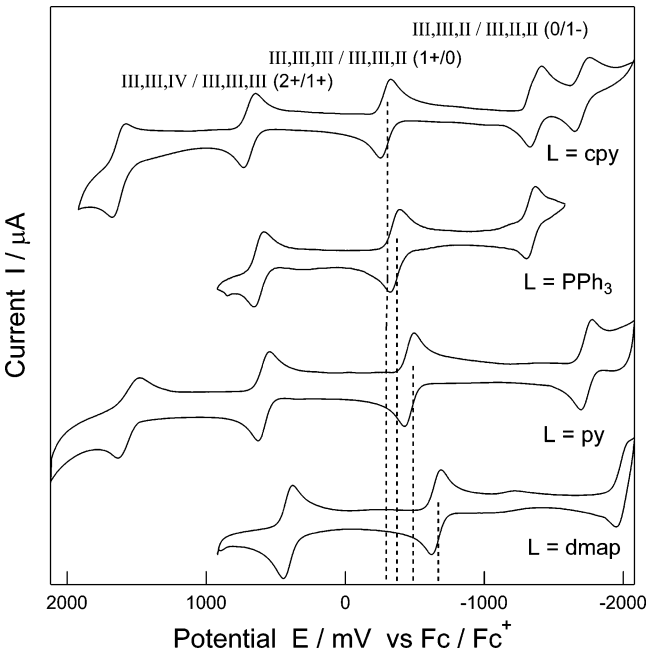

Figure 1. Cyclic voltammograms of a series of $[Ru_3(\mu_3\text{-}O)(\mu\text{-}CH_3CO_2)_6L_3]PF_6$ in AN containing 0.1 M $(n\text{-}C_4H_9)_4NPF_6$ as a supporting electrolyte at a scan rate of 100 mV^{-1}. Roman numerals indicate the formal oxidation number of three Ru ions, and Arabic numerals indicate the total charge.

The free-energy change of the radical ion pair (ΔG_{RIP}) was evaluated from the Rehm−Weller eq 1[32] using the E_{red} value of $[Ru_3(\mu_3\text{-}O)(\mu\text{-}CH_3CO_2)_6L_3]PF_6$ and oxidation potential (E_{ox}) of electron-donors

$$\Delta G_{RIP} = E_{ox} - E_{red} - E_c \qquad (1)$$

where E_c refers to Coulomb energy as calculated by eq 2

$$E_c \text{ (in eV)} = (z_{D+}z_{A-})e^2/23.06 \times d_{cc}\epsilon_s \qquad (2)$$

where z_{D+} and z_{A-} refer to the effective charge of D and A, respectively; d_{cc} refers to collision radius between the two moieties; ϵ_s refers to static dielectronic constant of the solvent used for the rate constant and the redox potential measurements. The evaluated ΔG_{RIP} values in AN are summarized in Table 1.

(28) Walsh, J. L.; Baumann, J. A.; Meyer, T. J. *Inorg. Chim. Acta* **1980**, *19*, 2145−2151.
(29) Toma, H. E.; Cunha, C. J.; Cipriano, C. *Inorg. Chim. Acta* **1988**, *154*, 63−66.
(30) Toma, H. E.; Araki, K.; Alexiou, A. D. P.; Nikolaou, S.; Dovidauskas, S. *Coord Chem. Rev.* **2001**, *219*−*221*, 187−234.
(31) Jones, S. W.; Jordan, M. R.; Brewer, K. J. *Molecular and Supramolecular Photochemistry*; Ramamurthy, V., Schanze, K. S., Eds.; Marcel Dekker: New York, 1999; Vol. 4, Chapter 4.
(32) Rehm, D.; Weller, A. *Isr. J. Chem.* **1970**, *8*, 259−271.

Table 1. Absorption Spectral Data and Reduction Potential (E_{red}) of $[Ru_3(\mu_3\text{-}O)(\mu\text{-}CH_3CO_2)_6L_3]^{+/0}$, p$K_a$ of Ligand, and Free-Energy Change for Radical Ion-Pair (ΔG_{RIP}) in AN

L	λ_{max}/nm (ϵ (M^{-1} cm^{-1})) $[Ru(\mu_3\text{-}O)(\mu\text{-}CH_3CO_2)_6(L)_3]^+$	λ_{max}/nm (ϵ (M^{-1} cm^{-1})) $[Ru(\mu_3\text{-}O)(\mu\text{-}CH_3CO_2)_6(L)_3]^0$	pK_a	E_{red}/V (+/0)[a] vs Fc/Fc^+	ΔG_{RIP}/eV ZnTPP, ZnTBPc
cpy	705(6600)/379(11400)	943(11400)/480(14500)	1.7	−0.27	0.64, 0.30
PPh_3	738(5500)/410(7400)	985(7900)/345(15100)	2.6	−0.35	0.72, 0.39
py	692(5600)/322(8900)	920(9000)/391(11800)	5.2	−0.46	0.84, 0.51
dmap	685(8200)/419(7900)	926(11800)/343(29000)	9.7	−0.65	1.02, 0.69

[a] E_{red} values were obtained from $(E_{pa} + E_{pc})/2$, where E_{pa} and E_{pc} are referred to peaks of anodic and cathodic scan vs Fc/Fc^+, respectively. E_{ox} values for ZnTPP and ZnTBPc were 0.38 and 0.04 V vs Fc/Fc^+ in AN.

Table 2. Free Energy Changes ($-\Delta G_{ET}^T$), Quenching Rate Constants (k_q), Quantum Yields (Φ_{ET}), and Electron-Transfer Rate-Constant (k_{ET}) for Electron-Transfer Processes of ^{3}ZnTPP* and $[Ru_3(\mu_3\text{-}O)(\mu\text{-}CH_3CO_2)_6L_3]PF_6$ and Free-Energy Changes ($-\Delta G_{BET}$) and Rate Constants (k_{BET}^{second}) for Back Electron-Transfer

L	solvent	$-\Delta G_{ET}^T$ [a]/eV	k_q/M^{-1} s^{-1}	Φ_{ET}[b]	k_{ET}/M^{-1} s^{-1}	$-\Delta G_{BET}$/eV	k_{BET}^{second}/M^{-1} s^{-1}
cpy	AN	0.89	8.0×10^9	0.30	2.4×10^9	0.64	9.4×10^9
PPh_3		0.81	9.3×10^9	0.23	2.1×10^9	0.72	1.1×10^{10}
py		0.69	8.0×10^9	0.21	1.7×10^9	0.84	1.7×10^{10}
dmap		0.51	8.4×10^9	<0.1	$<8.4 \times 10^8$	1.02	(2.2×10^{10})[c]
cpy	BN	0.87	1.9×10^9	0.24	4.6×10^8	0.66	3.4×10^9
PPh_3		0.78	2.3×10^9	0.18	4.1×10^8	0.75	4.2×10^9
py		0.66	2.0×10^9	0.16	3.2×10^8	0.87	7.3×10^9
dmap		0.47	1.9×10^9	< 0.1	$<1.9 \times 10^8$	1.06	(7.6×10^9)[c]
cpy	DCB	0.81	1.9×10^9	0.21	4.0×10^8	0.72	4.3×10^9
PPh_3		0.72	1.9×10^9	0.17	3.2×10^8	0.81	6.4×10^9
py		0.59	2.1×10^9	0.15	3.1×10^8	0.94	5.2×10^9
dmap		0.41	2.1×10^9	<0.1	$<2.1 \times 10^7$	1.12	(7.6×10^9)[c]

[a] Energy level (E_0) of ^{3}ZnTTP* was 1.53 eV.[36] [b] The ϵ value for ^{3}ZnTPP* is 8.2×10^3 M^{-1} cm^{-1} at 840 nm.[36] [c] Estimation was difficult due to weak signal.

Table 3. Free-Energy Changes ($-\Delta G_{ET}^T$), Quenching Rate Constants (k_q), Quantum Yields (Φ_{ET}), and Electron-Transfer Rate-Constant (k_{ET}) for Electron-Transfer Processes of ^{3}ZnTBPc* and $[Ru_3(\mu_3\text{-}O)(\mu\text{-}CH_3CO_2)_6L_3]PF_6$ and Free-Energy Changes ($-\Delta G_{BET}$)

L	solvent	$-\Delta G_{ET}^T$ [a]/eV	k_q/M^{-1} s^{-1}	Φ_{ET}[b]	k_{ET}/M^{-1} s^{-1}	$-\Delta G_{BET}$/eV	k_{BET}^{second}/M^{-1} s^{-1}
cpy	AN	0.83	9.3×10^9	0.69	6.4×10^9	0.30	2.2×10^9
PPh_3		0.74	9.8×10^9	0.33	3.2×10^9	0.39	2.9×10^9
py		0.62	9.8×10^9	0.18	1.8×10^9	0.51	3.8×10^9
dmap		0.44	7.3×10^9	<0.1	$<7.8 \times 10^8$	0.69	(3.9×10^9)[c]
cpy	BN	0.81	3.2×10^9	0.66	2.1×10^9	0.32	1.5×10^9
PPh_3		0.73	3.5×10^9	0.30	1.0×10^9	0.40	1.7×10^9
py		0.59	3.4×10^9	0.20	5.4×10^8	0.54	2.4×10^9
dmap		0.41	3.7×10^9	<0.1	$< 3.7 \times 10^8$	0.72	(3.4×10^9)[c]
cpy	DCB	0.80	2.1×10^9	0.68	1.4×10^9	0.33	1.4×10^9
PPh_3		0.73	2.4×10^9	0.27	6.5×10^8	0.40	1.5×10^9
py		0.59	2.2×10^9	0.25	5.5×10^8	0.54	3.0×10^9
dmap		0.41	2.1×10^9	<0.1	$<2.1 \times 10^8$	0.72	(3.2×10^9)[c]

[a] Energy level (E_0) of ^{3}ZnTBPc* (1.13 eV).[37] [b] The ϵ value for ^{3}ZnTBPc* is 4.9×10^4 M^{-1} cm^{-1} at 480 nm.[37] [c] Estimation was difficult due to weak signal.

Free-energy changes for electron transfer (ΔG_{ET}) were calculated by eq 3

$$\Delta G_{ET} = \Delta G_{RIP} - E_0 \quad (3)$$

where E_0 refers to the energy of the lowest excited state of the photosensitizer, from which electron transfer occurs. As shown in the later section in this paper, electron transfer was proved to occur from the excited triplet states of ZnTPP and ZnTBPc, for which the energy levels of the lowest triplet states were employed as E_0.[36,37] In Tables 2 and 3, the ΔG_{ET}^T values via ^{3}ZnTPP* and ^{3}ZnTBcP* are listed, respectively.

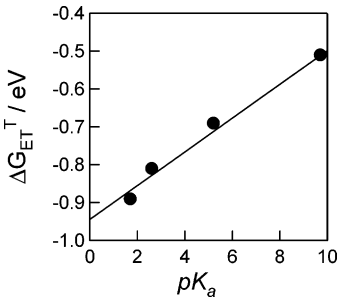

Figure 2. Plots of the $-\Delta G_{ET}^T$ for electron transfer between the $[Ru_3(\mu_3\text{-}O)(\mu\text{-}CH_3CO_2)_6L_3]PF_6$ and ZnTPP vs pK_a in AN.

In Figure 2, the ΔG_{ET}^T values via ^{3}ZnTPP* are plotted vs pK_a values of the ligands. With a decrease of pK_a, the calculated $-\Delta G_{ET}^T$ values increase monotonically. Therefore,

(33) Davis, S.; Drago, R. S. *Inorg. Chem.* **1988**, *27*, 4759−4760.
(34) Abe, M.; Sasaki, Y.; Yamaguchi, T.; Ito, T. *Bull. Chem. Soc. Jpn.* **1992**, *65*, 1585−1590.
(35) Cotton, F. A.; Norman, J. G., Jr. *Inorg. Chim. Acta* **1972**, *6*, 411−419.
(36) Murov, S. L.; Carmichael, I.; Hug, G. L. *Handbook of Photochemistry*, 2nd ed.; Marcel Dekker: New York, 1993.
(37) Lawrence, D. S.; Whitten, D. G. *Photochem. Photobiol.* **1996**, *64*, 923−935.

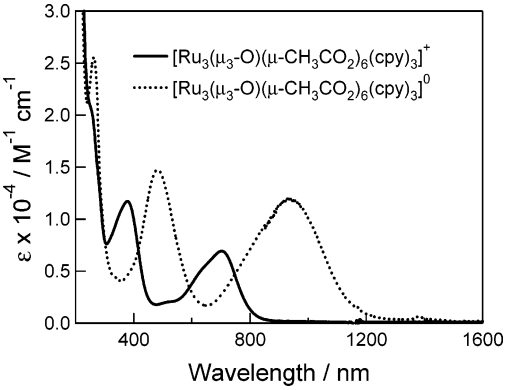

Figure 3. Absorption spectral changes obtained by controlling potentials, at 0 V for $[Ru_3(\mu_3\text{-}O)(\mu\text{-}CH_3CO_2)_6(cpy)_3]PF_6$ and at −500 mV for $[Ru_3(\mu_3\text{-}O)(\mu\text{-}CH_3CO_2)_6(cpy)_3]^0$ in AN containing 0.1 M $(n\text{-}C_4H_9)_4NPF_6$.

smaller values of pK_a increase the exothermicity of the electron-transfer process.

Steady-State Absorption Spectra. As shown in Figure 3, characteristic absorption bands of $[Ru_3(\mu_3\text{-}O)(\mu\text{-}CH_3CO_2)_6(cpy)_3]PF_6$ were observed at 379 and 705 nm by controlled-potential at 0 V. By applying negative potential at −500 mV, new absorption bands appeared at 480 and 943 nm, which are attributed to the reduced form, $[Ru_3(\mu_3\text{-}O)(\mu\text{-}CH_3CO_2)_6(cpy)_3]^0$. The absorption bands in the longer wavelength region are attributed to the d−d transition, while the absorption bands in the shorter wavelength are ascribed to the cluster to ligand charge-transfer transition (CLCT), and the third absorption band shorter than 350 nm is assigned to a $\pi-\pi^*$ transition of the ligand.[10,33−35] The shifts of the absorption peaks of $[Ru_3(\mu_3\text{-}O)(\mu\text{-}CH_3CO_2)_6(cpy)_3]^0$ to the longer wavelength region compared with the corresponding peaks of $[Ru_3(\mu_3\text{-}O)(\mu\text{-}CH_3CO_2)_6(cpy)_3]^+$ were well explained in the literature.[10,30,35]

The absorption peaks before and after applying negative electric potentials −300 to −700 mV are summarized in Table 1. The extinction coefficients (ϵ) of $[Ru_3(\mu_3\text{-}O)(\mu\text{-}CH_3CO_2)_6(L)_3]^0$ were determined by comparison with the consumption of $[Ru_3(\mu_3\text{-}O)(\mu\text{-}CH_3CO_2)_6(L)_3]PF_6$. Since these absorption bands are dramatically affected by the overall charge (formal oxidation state), it would be expected that the photoinduced electron transfer can be easily monitored with using the transient absorption spectra by monitoring the absorption bands in the visible and near-IR regions.

Photoinduced Electron-Transfer Processes. By the excitation of ZnTPP in the presence of $[Ru_3(\mu_3\text{-}O)(\mu\text{-}CH_3CO_2)_6(cpy)_3]PF_6$ in deaerated AN with the laser light at 532 nm which predominantly excites ZnTPP (Supporting Information, Figure S1), the transient absorption spectra in the visible and near-IR regions were observed as shown in Figure 4. Immediately after the laser light pulse, the transient absorption bands appeared at 470 and 840 nm which can be attributed to ^{3}ZnTPP*.[36] With concomitant decay of ^{3}ZnTPP*, new absorption bands appeared at 900 and 650 nm, which are assigned to the absorption bands of $[Ru_3(\mu_3\text{-}O)(\mu\text{-}CH_3CO_2)_6(cpy)_3]^0$ and $ZnTPP^{\bullet+}$, respectively. The absorption time profiles (inset of Figure 4) show that the rise of the absorption band of $[Ru_3(\mu_3\text{-}O)(\mu\text{-}CH_3CO_2)_6(cpy)_3]^0$ at 900

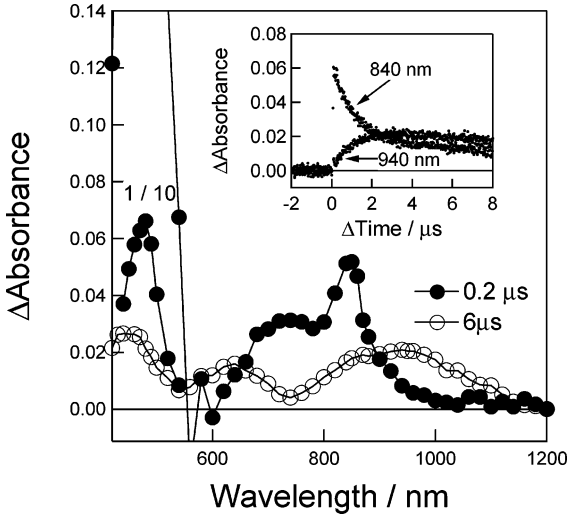

Figure 4. Transient absorption spectra obtained by 532 nm laser photolysis of ZnTPP (0.05 mM) in the presence of $[Ru_3(\mu_3\text{-}O)(\mu\text{-}CH_3CO_2)_6(cpy)_3]PF_6$ (0.1 mM) in Ar-saturated AN: (●) 0.2 μs and (○) 6 μs. Inset: Absorption−time profiles at 840 and 940 nm.

nm was almost a mirror image with the decay of ^{3}ZnTPP* at 850 nm. Thus, it was clearly indicated that photoinduced electron-transfer occurs via ^{3}ZnTPP* as shown in eq 4.

$$^3ZnTPP^* + [Ru_3(\mu_3\text{-}O)(\mu\text{-}CH_2CO_2)_6L_3]^+ \rightarrow ZnTPP^{\bullet+} + [Ru_3(\mu_3\text{-}O)(\mu\text{-}CH_2CO_2)_6L_3]^0 \quad (4)$$

To confirm the transient species produced by the photolysis of $[Ru_3(\mu_3\text{-}O)(\mu\text{-}CH_3CO_2)_6(cpy)_3]PF_6$, we tried to observe the transient absorption spectrum by the nanosecond laser excitation of $[Ru_3(\mu_3\text{-}O)(\mu\text{-}CH_3CO_2)_6(cpy)_3]PF_6$; however, no appreciable absorption band appeared as shown in Supporting Information (Figure S2). Furthermore, the contribution of the singlet excited state of ZnTPP (^{1}ZnTPP*) to the electron-transfer process was considered to be small, because the concentrations of $[Ru_3(\mu_3\text{-}O)(\mu\text{-}CH_3CO_2)_6(cpy)_3]PF_6$ employed in the present study were too low to quench the fluorescence of ZnTPP.

In the case of ^{3}ZnTBPc*, transient absorption spectra were obtained by the 532 nm laser light excitation of ZnTBPc in the presence of $[Ru_3(\mu_3\text{-}O)(\mu\text{-}CH_3CO_2)_6(cpy)_3]PF_6$ in deaerated AN as shown in Figure 5. The absorption band appeared at 480 nm after laser excitation was attributed to ^{3}ZnTBPc*.[37] With the decay of ^{3}ZnTBPc*, the absorption bands appeared at 840 and 900 nm, which are assigned to $ZnTBPc^{\bullet+}$ and $[Ru_3(\mu_3\text{-}O)(\mu\text{-}CH_3CO_2)_6(cpy)_3]^0$, respectively.[38] The inserted time profile in Figure 5 shows that $ZnTBPc^{\bullet+}$ and $[Ru_3(\mu_3\text{-}O)(\mu\text{-}CH_3CO_2)_6(cpy)_3]^0$ increase with the decay of ^{3}ZnTBPc*. The absorbance at 480 nm did not decay completely in the longer time region, because the absorption band of $ZnTBPc^{\bullet+}$ and the CLCT band of $[Ru_3(\mu_3\text{-}O)(\mu\text{-}CH_3CO_2)_6(cpy)_3]^0$ may be overlapping with that of ^{3}ZnTBPc*. The rise curves of $ZnTBPc^{\bullet+}$ and $[Ru_3(\mu_3\text{-}O)(\mu\text{-}CH_3CO_2)_6(cpy)_3]^0$ seem to be mirror images with the decay curve of ^{3}ZnTBPc*, indicating

(38) Nyokong, T.; Gasyna, Z.; Stillman, M. J. *Inorg. Chem.* **1987**, *26*, 548−553.

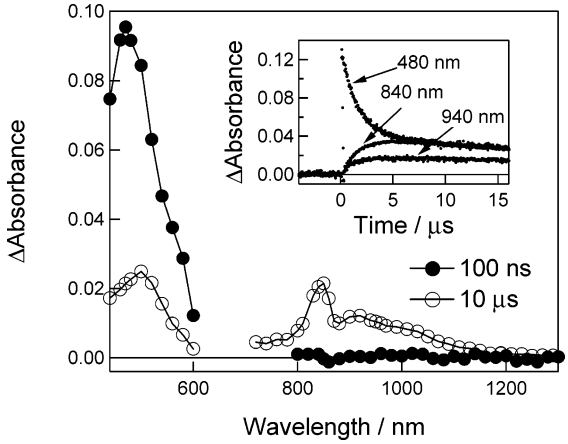

Figure 5. Transient absorption spectra obtained by 532 nm laser photolysis of ZnTBPc (0.05 mM) in the presence of $[Ru_3(\mu_3\text{-}O)(\mu\text{-}CH_3CO_2)_6(cpy)_3]\text{-}PF_6$ (0.1 mM) in Ar-saturated BN: (●) 0.1 μs and (○) 10 μs. Inset: Absorption−time profiles at 480, 840, and 940 nm, respectively.

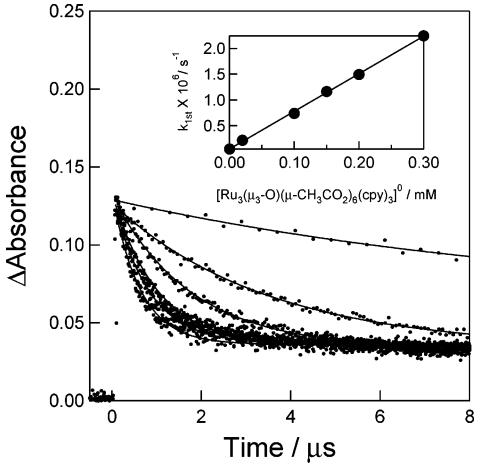

Figure 6. Decay time profile of ^{3}ZnTBPc* at 480 nm with changing concentration of $[Ru_3(\mu_3\text{-}O)(\mu\text{-}CH_3CO_2)_6(cpy)_3]PF_6$ (from upper, 0, 0.02, 0.10, 0.15, 0.20, and 0.30 mM). Inset: Pseudo-first-order plot.

that photoinduced electron-transfer occurs via ^{3}ZnTBPc* as shown in eq 5.

$$^3\text{ZnTBPc}^* + [Ru_3(\mu_3\text{-}O)(\mu\text{-}CH_3CO_2)_6L_3]^+ \rightarrow \text{ZnTBPc}^{\bullet+} + [Ru_3(\mu_3\text{-}O)(\mu\text{-}CH_2CO_2)_6L_3]^0 \quad (5)$$

Rates and Efficiencies of Electron Transfer. The decay curves of ^{3}ZnTTP* and ^{3}ZnTBPc* in the insets of Figures 4 and 5 obeyed first-order kinetics under the condition of $[^3\text{ZnTBPc}^*] \ll [Ru_3(\mu_3\text{-}O)(\mu\text{-}CH_3CO_2)_6L_3]PF_6$. The observed first-order rate constants (k_{obs}) increase linearly with the concentration of $[Ru_3(\mu_3\text{-}O)(\mu\text{-}CH_3CO_2)_6L_3]PF_6$ as shown in Figure 6. The slopes of the pseudo-first-order plots yield the second-order rate constant (k_q) for bimolecular quenching of ^{3}ZnTTP* or ^{3}ZnTBPc* with $[Ru_3(\mu_3\text{-}O)(\mu\text{-}CH_3CO_2)_6L_3]\text{-}PF_6$. The k_q values were evaluated in the order of 10^9 M^{-1} s^{-1} as listed in Tables 2 and 3. For the same ligand and solvent, the k_q values for ^{3}ZnTTP* are almost the same as those of ^{3}ZnTBPc*. For the same solvent, the k_q values are almost the same with the change of the ligands, while the k_q values are solvent dependent. In the present study, we used three solvents, which have the following properties: highly polar AN ($\epsilon_s = 37.5$) with less viscosity ($\eta = 0.325$), polar BN ($\epsilon_s = 25.2$ and $\eta = 1.111$), and moderately polar solvent DCB ($\epsilon_s = 9.9$ and $\eta = 1.202$).[36] Since the ΔG_{ET} values are sufficiently negative (Tables 2 and 3), the k_q values should be close to the diffusion-controlled limit (k_{diff}),[36] which depends on the solvent viscosity, although the estimated k_q values in three solvents are smaller than the k_{diff} values by a factor of $^1/_2$−$^1/_3$.

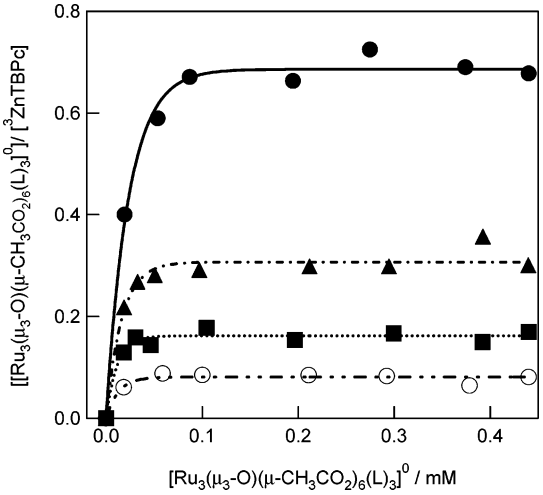

Figure 7. Plots of $[[Ru_3(\mu_3\text{-}O)(\mu\text{-}CH_3CO_2)_6(L)_3]^0]/[^3\text{ZnTBPc}^*]$ vs $[[Ru_3(\mu_3\text{-}O)(\mu\text{-}CH_3CO_2)_6(L)_3]PF_6]$: for ligands, cpy (●), PPh_3 (▲), py (■), and dmap (○).

The efficiency of electron-transfer can be calculated from the ratio of the maximal concentration of the generated $[Ru_3(\mu_3\text{-}O)(\mu\text{-}CH_3CO_2)_6L_3]^0$ (abbreviated as $[(Ru_3)^0]_{max}$) to the initial concentration of ^{3}ZnTPP* or ^{3}ZnTBPc* (abbreviated as $[^3\text{ZnP}^*]_{init}$), which are calculated by employing the observed absorbance and molar extinction coefficient (Table 1). The ratios are plotted against $[Ru_3(\mu_3\text{-}O)(\mu\text{-}CH_3CO_2)_6L_3]^+$ as shown in Figure 7, in which the ratios saturate at the higher concentration of $[Ru_3(\mu_3\text{-}O)(\mu\text{-}CH_3CO_2)_6L_3]^+$ than at 0.1 mM.[39,40]

In general, the ratio can be expressed as a function of the concentration of $[Ru_3(\mu_3\text{-}O)(\mu\text{-}CH_3CO_2)_6L_3]PF_6$ as shown by eq 6[41]

$$[(Ru_3)^0]_{max}/[^3\text{ZnP}^*]_{init} = k_{ET}[(Ru_3)^+]/\{k_T + k_q[(Ru_3)^+]\} \quad (6)$$

where k_{ET} refers to electron-transfer rate-constant via ^{3}ZnTPP* or ^{3}ZnTBPc* and k_T to the intrinsic decay of ^{3}ZnTPP* or ^{3}ZnTBPc* in the absence of $[Ru_3(\mu_3\text{-}O)(\mu\text{-}CH_3\text{-}CO_2)_6L_3]PF_6$. Since $k_T \ll k_q[(Ru_3)^+]$ as shown in Figure 6, the right term of eq 6 becomes constant, k_{ET}/k_q. The saturated value is defined as the quantum yield for electron-transfer (Φ_{ET}) via ^{3}ZnTPP or ^{3}ZnTBPc*. The Φ_{ET} values are less

(39) Nojiri, T.; Alam, M. M.; Konami, H.; Watanabe, A.; Ito, O. *J. Phys. Chem. B* **1997**, *101*, 7943−7947.
(40) Itou, M.; Fujitsuka, M.; Araki, Y.; Ito, O.; Kido, H. *J. Porphyrins Phthalocyanines* **2003**, *7*, 405−414.
(41) Yamanaka, K.; Fujitsuka, M.; Ito, O.; Aoshima, T.; Fukushima, T.; Miyashi, T. *Bull. Chem. Soc. Jpn.* **2003**, *76*, 1341−1349.

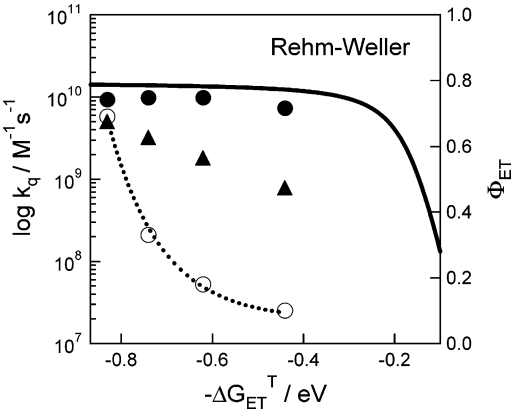

Figure 8. Plots of log k_q (●), log k_{ET} (▲), and Φ_{ET} (○) vs $-\Delta G_{ET}^{T}$ for ^{3}ZnTPP* in AN; solid curve is obtained by Rehm−Weller equation.

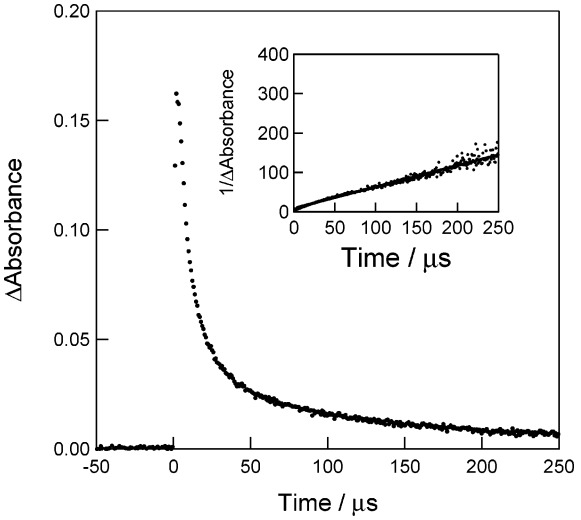

Figure 9. Second-order plot for the decay of $[Ru_3(\mu_3\text{-O})(\mu\text{-CH}_3CO_2)_6(cpy)_3]^0$ at 940 nm in the presence of $ZnTPP^{\bullet+}$ in deaerated AN. Inset: Time profile.

than ca. 0.7, which indicates that amounts $(1 - \Phi_{ET})$ of ^{3}ZnTPP* and ^{3}ZnTBPc* are deactivated without electron transfer (Tables 2 and 3). The Φ_{ET} values via ^{3}ZnTBPc* are higher than those via ^{3}ZnTPP* for the same ligand and solvent. The Φ_{ET} values were increased with the electron withdrawing ability of ligands: cpy > PPh_3 > py > dmap.

The k_{ET} value of the electron-transfer process was estimated from a relation, $k_{ET} = k_q \times \Phi_{ET}$; thus, the k_{ET} values are less than the k_q values, because the Φ_{ET} values are less than ca. 0.7. The k_{ET} values via ^{3}ZnTBPc* are larger than those via ^{3}ZnTTP*, which is mainly determined by the larger Φ_{ET} via ^{3}ZnTBPc*, because the k_q values are almost the same for both ^{3}ZnTPP* and ^{3}ZnTBPc*. The k_{ET} values increase with the electron withdrawing ability of ligands in the same order as the Φ_{ET} value.

To clarify the ligand effect, the k_q (●), k_{ET} (○), and Φ_{ET} (▲) values for ^{3}ZnTBPc* in AN are plotted against the ΔG_{ET}^{T} values as shown in Figure 8. The k_q values are invariant with the ΔG_{ET}^{T} values, since the ΔG_{ET}^{T} values are all sufficiently negative and approach the k_{diff} values as predicted by the semiempirical Rehm−Weller equation.[32] On the other hand, the Φ_{ET} values drastically decrease with an increase in the ΔG_{ET}^{T} values, which are strongly dependent on the pK_a value of the ligands. Thus, the k_{ET} values are appreciably dependent on the electron-withdrawing ability of the ligands.

In general, the Φ_{ET} and k_{ET} values are strongly affected by the solvent polarity; however, the Φ_{ET} and k_{ET} values in AN are only slightly larger than those in BN and DCB. The small solvent effect of our electron-transfer systems can be attributed to the small Coulombic term between the radical cations of donors and neutral Ru cluster in the electron transfer state. Such a small dependence of the solvent polarity is rather advantageous for constructing the photoinduced electron-transfer devices in films and solids.

Back Electron-Transfer Processes. In the long time scale measurements, the transient absorption bands due to $[Ru_3(\mu_3\text{-O})(\mu\text{-CH}_3CO_2)_6(cpy)_3]^0$ showed slow decay after reaching maximal concentration as shown in Figure 9. Similar slow decay was observed for $ZnTPP^{\bullet+}$. Such a slow decay of $[Ru_3(\mu_3\text{-O})(\mu\text{-CH}_3CO_2)_6L_3]^0$ obeyed second-order kinetics, which indicates that $[Ru_3(\mu_3\text{-O})(\mu\text{-CH}_3CO_2)_6L_3]^0$ and $ZnTPP^{\bullet+}$ are diminished by the back electron transfer after solvation as free ions (eq 7).[42,43]

$$ZnTPP^{\bullet+} + [Ru_3(\mu_3\text{-O})(\mu\text{-CH}_2CO_2)_6L_3]^0 \xrightarrow{k_{BET}^{2nd}} ZnTPP + [Ru_3(\mu_3\text{-O})(\mu\text{-CH}_2CO_2)_6L_3]^+ \quad (7)$$

The slope of the line in Figure 9 gave the ratio $(2k_{BET}/\epsilon_0)$, in which ϵ_0 denotes the molar extinction coefficients of $[Ru_3(\mu_3\text{-O})(\mu\text{-CH}_3CO_2)_6L_3]^0$. On employing the ϵ_0 values for $[Ru_3(\mu_3\text{-O})(\mu\text{-CH}_3CO_2)_6L_3]^0$ (in Table 1), the k_{BET}^{second} values were evaluated to be $(0.3-1.7) \times 10^{10}$ M^{-1} s^{-1} as listed in Table 2. The k_{BET}^{second} values were all close to the k_{diff} values,[36] which supports that the back electron-transfer process is endothermic as anticipated from the free-energy change of the back electron-transfer process (ΔG_{BET}), which is equal to $-\Delta G_{RIP}$ as listed in Table 2.

$$\Delta G_{BET} = -\Delta G_{RIP} \quad (8)$$

For $ZnTBPc^{\bullet+}$, similarly slow decays of $[Ru_3(\mu_3\text{-O})(\mu\text{-CH}_3CO_2)_6L_3]^0$ were observed and the values of k_{BET}^{second} for the systems of $[Ru_3(\mu_3\text{-O})(\mu\text{-CH}_3CO_2)_6L_3]^0$ and $ZnTBPc^{\bullet+}$ were evaluated in the region of $(1-4) \times 10^9$ M^{-1} s^{-1} (Table 3), which are slightly smaller than those of $ZnTPP^{\bullet+}$. This trend may be related to the small ΔG_{BET} for $ZnTBPc^{\bullet+}$ compared with those for $ZnTPP^{\bullet+}$, suggesting that the back electron-transfer process is in the normal region of the Marcus parabola.[44]

Energy Diagram. The energy diagram for electron- and energy-transfer processes is schematically illustrated in Figure 10 for ZnTPP and ZnTBPc, in which the energy values were calculated relative to the ground state. The

(42) Ito, O.; Sasaki, Y.; Yoshikawa, Y.; Watanabe, A. *J. Phys. Chem.* **1995**, *99*, 9838−9842.
(43) Fujitsuka, M.; Luo, C.; Ito, O. *J. Phys. Chem. B* **1999**, *103*, 445−449.
(44) (a) Marcus, R. A.; Sutin, N. *Biochim. Biophys. Acta* **1985**, *811*, 265−322. (b) Marcus, R. A. *Angew. Chem., Int. Ed.* **1993**, *32*, 1111−1121.

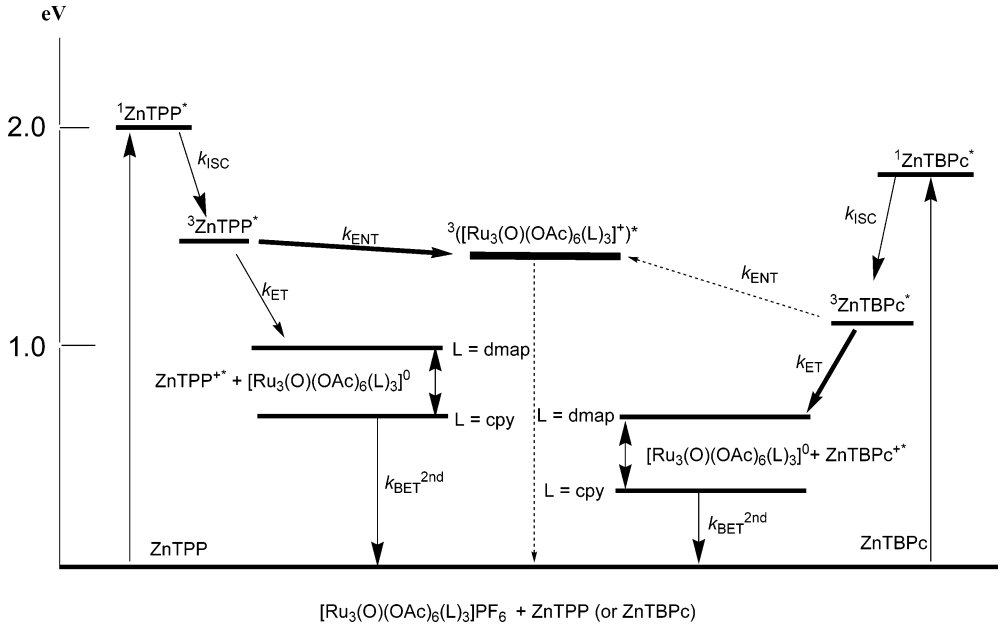

Figure 10. Schematic energy diagram for electron-transfer processes via ^{3}ZnTPP* and ^{3}ZnTBPc* in AN. [Ru$_3$(μ_3-O)(μ-CH$_3$CO$_2$)$_6$(L$_3$)] is abbreviated as [Ru$_3$(O)(OAc)$_6$L$_3$].

energies of the triplet states of [Ru$_3$(μ_3-O)(μ-CH$_3$CO$_2$)$_6$L$_3$]-PF$_6$ are evaluated to be 1.48 eV from the phosphorescence spectra (Supporting Information, Figure S3); solvent effect and ligand effect on these energy levels of the excited triplet states of [Ru$_3$(μ_3-O)(μ-CH$_3$CO$_2$)$_6$L$_3$]PF$_6$ were small. From this energy diagram, electron transfer via ^{3}ZnTPP* (E_0 = 1.53 eV) may take place competitively with energy-transfer process (k_{ENT}) from ^{3}ZnTPP* to [Ru$_3$(μ_3-O)(μ-CH$_3$CO$_2$)$_6$-(cpy)$_3$]PF$_6$. On the other hand, since energy transfer from ^{3}ZnTBPc* to [Ru$_3$(μ_3-O)(μ-CH$_3$CO$_2$)$_6$L$_3$]PF$_6$ is uphill, electron transfer predominantly occurs. Thus, the Φ_{ET} the k_{ET} values from ^{3}ZnTBPc* (E_0 = 1.13 eV) to [Ru$_3$(μ_3-O)(μ-CH$_3$-CO$_2$)$_6$L$_3$]PF$_6$ are larger than those from ^{3}ZnTPP*; nevertheless, the ΔG_{ET}^T values are almost the same for ZnTPP and ZnTBPc. The variation of the Φ_{ET} and k_{ET} values by changing the ligands can be considered to depend on the thermodynamic parameters.

Conclusion

In the present study of photoinduced electron-transfer involving oxo-acetato-bridged triruthenium cluster, [Ru$_3$(μ_3-O)(μ-CH$_3$CO$_2$)$_6$L$_3$]$^{+/0}$, having characteristic absorption bands in the visible and near-IR regions, we proved that application of the laser flash photolysis measuring the transient spectra in this wavelength region was quite useful. For the triplet excited photosensitizing donors, ZnTPP and ZnTBPc, the [Ru$_3$(μ_3-O)(μ-CH$_3$CO$_2$)$_6$L$_3$]$^+$ acts as a good electron acceptor whose properties are controlled by several terminal ligands and solvent polarities. The systems employed in this study show reversible processes which mean that they could be useful in building photosensitizing and electron mediation systems to convert photoenergy to chemical energy or electric energy.

Acknowledgment. This research was partially supported by a Grant-in-Aid for the COE project, Giant Molecules and Complex Systems, 2002. This work was also supported by a Grant-in-Aid for Scientific Research on Priory Area (417) from the Ministry of Education, Culture, Sports, Science, and Technology (NEXT) of Japanese Government.

Supporting Information Available: Absorption spectra of ZnTPP and ZnTBPc, nanosecond transient absorption spectra of [Ru$_3$(μ_3-O)(μ-CH$_3$CO$_2$)$_6$(py)$_3$]PF$_6$ in AN, and phosphorescence spectra of [Ru$_3$(μ_3-O)(μ-CH$_3$CO$_2$)$_6$L$_3$]PF$_6$. This material is available free of charge via the Internet at http://pubs.acs.org.

IC049114S